



18th International Conference Metal Forming 2020

# Flexible 3D stretch bending of aluminium alloy profiles: an experimental and numerical study

Torgeir Welo<sup>a,\*</sup>, Jun Ma<sup>a</sup>, Jørgen Blindheim<sup>a</sup>, Taekwang Ha<sup>a</sup>, Geir Ringen<sup>a</sup>

<sup>a</sup>*Department of Mechanical and Industrial Engineering, Norwegian University of Science and Technology, Trondheim, 7491, Norway*

\* Corresponding author. Tel.: +47-41440061. E-mail address: [torgeir.welo@ntnu.no](mailto:torgeir.welo@ntnu.no)

## Abstract

Three-dimensionally (3D) shaped extrusions are attracting increased attention in order to meet the ever-growing demands on weight reduction to obtain lower emissions in the automobile industry. With the current transformation towards Industry 4.0, the metal forming sector is currently undergoing rapid changes. Improved flexibility of product, process, and machine tools is one of the strategic points for more efficient manufacturing process. Aiming at this goal, this paper introduces a new, flexible stretch bending technology for forming of complex 3D extruded profiles. This innovation is based on adding the number of axes combined with a tooling concept utilizing part-specific inserts, thus enabling the manufacture of different geometrical configurations with low tool investments. In addition, multi-functional sensors are integrated into the machine and tool system, providing the possibility of real-time and in-process control of the forming process. To verify the capabilities of the new 3D stretch bending process, a full-scale machine is designed, built and installed in a laboratory to conduct closely-controlled 2D and 3D bending experiments. Furthermore, a finite element (FE) model is established to study mechanisms associated with elastic springback control. The deformation history characteristics and springback behavior are analyzed to provide in-depth understanding of the flexible stretch bending process and the mechanisms involved.

© 2020 The Authors. Published by Elsevier B.V.

This is an open access article under the CC BY-NC-ND license (<http://creativecommons.org/licenses/by-nc-nd/4.0/>)  
Peer-review under responsibility of the scientific committee of the 18th International Conference Metal Forming 2020

*Keywords:* 3D stretch bending, flexibility, profile, springback, finite element simulation

## 1. Introduction

With the current transformation to the Industry 4.0 era, the metal forming sector undergoes drastic changes. One of the crucial aspects of this revolution in manufacturing is to increase the flexibility of products, machines, and processes, to enable a shift from conventional mass production towards more on-demand type manufacturing for mass customization [1,2]. This need calls for the development of new innovative forming technologies.

Three-dimensionally (3D) shaped profiles are attracting more and more attention to meet the ever-growing demands on weight reduction to obtain lower emissions in the automobile industry [3, 4]. Improved flexibility of products, machines/tools and processes is one of the strategic points for better control of product quality and lower manufacturing cost to achieve improved competitiveness in a dynamic market. However, this presumes that the Industry 4.0 concept is taken from one being preached by management consultants to real-world implementation.

Bending-based forming technologies are commonly used for manufacturing of profile-like products. Up to now, a series of methods have been developed to address different requirements of such products; examples are given as rotary draw bending (RDB), stretch bending, three-roll bending (TRB), and the recently proposed, so-called torque superposed spatial bending (TSSB) [5-7]. Among these methods, the roll-based TSSB allows the bending of profiles with a wide range of cross-sections [7,8]. Its advantage is the kinematic adjustment of the bending contour, leading to higher flexibility and lower tool cost, making it attractive for small batch production. TRB has relatively good flexibility, too, providing a large range of possible geometries. For 3D shapes, however, TRB is mainly suitable for circular tubes [9]. For profiles with more complex shapes, like multi-functional aluminum extrusions, there exist major difficulties and restrictions, although countermeasures have been proposed to overcome some of the shortcomings [10]. RDB is normally selected to address the forming context with tight-radius bending and thin-walls, using rigid and flexible mandrels [6]. However, RDB only provides flexibility

2351-9789 © 2020 The Authors. Published by Elsevier B.V.

This is an open access article under the CC BY-NC-ND license (<http://creativecommons.org/licenses/by-nc-nd/4.0/>)  
Peer-review under responsibility of the scientific committee of the 18th International Conference Metal Forming 2020  
10.1016/j.promfg.2020.08.008

with regard to bending angle. RDB and TRB can be implemented on the same machine system to improve the forming capability of complex part configurations, as shown in Fig. 1.

Stretch bending is commonly based on the principle of form-closed forming. It is widely used to manufacture high-precision shapes for volume production in the automobile industry. The advantages of stretch bending are high shape accuracy and dimensional capabilities [4,11]. By applying superposition of tension and bending, global springback upon unloading can be minimized [12]. Still, some necessary trial-and-error attempts are usually needed to target the final part configuration relative to the shape of the die. Due to restrictions associated with the process kinematics, however, stretch bending enables large-radius bending only. Another challenge is high tool cost caused by its low part flexibility compared to other bending methods. In most cases, a set of tools can only support one target product, making it difficult to meet the flexibility requirements of, for example, a family of formed products. Attempts have been made, however, to improve the flexibility in stretch bending. For example, multi-point dies have been introduced to the stretch bending process [13–15]. By replacing rigid-geometry dies with multi-point dies, the shape flexibility can be improved to make the die surfaces reconfigurable in two planes to achieve 3D forming. Moreover, it can also facilitate local curvatures within a wide range along the length of the formed product. However, due to the discontinuous surface topology of multi-point dies, both the dimensional accuracy and surface quality are lower than in conventional stretch bending.

In conclusion, even though a number of bending processes has been developed and flexible design methods have been proposed for 3D bending, there is still a great need for new technologies that allow more complex and flexible part geometries, offering low manufacturing cost for individual products and product families. Moreover, better utilization of sensory input, as well as closed-loop-control, to improve the dimensional accuracy is another urgent issue that needs to be addressed to deliver increased value (-added) from the forming process.

In this paper, a new flexible stretch bending machine for producing complex 3D profiles is developed based on a novel design, utilizing multiple pivot axes, tooling inserts, and integrated multi-functional sensors. Both experiments and finite element (FE) numerical simulation of 2D and 3D stretch forming cases are carried out to test the capabilities of the new bending technology. Finally, the forming mechanism and springback behavior associated with the process is numerically studied to help understand the characteristics of the forming process.

The remainder of the paper is organized as follows: Section 2 presents the new bending technology developed. Section 3 introduces the experimental details and FE numerical modeling of the bending and unloading process. Section 4 presents the capability verification of the developed forming process and machine, along with FE-based analysis of forming characteristics and springback behavior. Finally, the conclusions are drawn in Section 5.

## 2. Flexible 3D Stretch Bending Process

In order to meet today's rapidly changing demands for more complex product geometries with high dimensional accuracy, a new flexible stretch bending technology is developed for manufacturing of both 2D and 3D shapes. Fig. 1 presents a schematic view of the bending method. The machine design is based on the theory of 3D bending previously reported in reference [11]. By designing a machine with multiple axes, the flexibility can be increased to accommodate the increased geometrical complexity of the product. Furthermore, by integrating a wide range of sensors as well as high-resolution drives and actuators, real-time and in-process adaptability, this can provide additional capability to use and control the inputs and variables — both upstream and in-process ones.

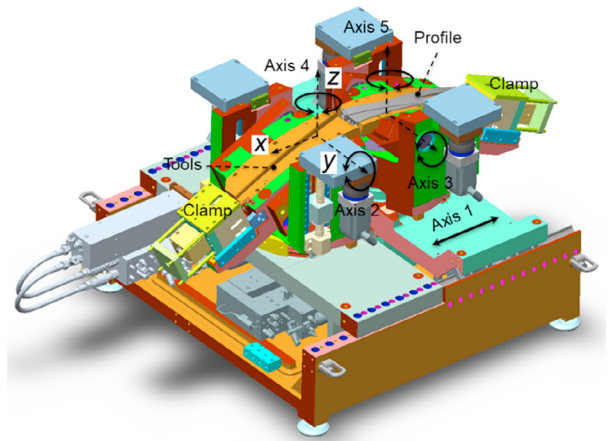


Fig. 1. Schematic view of the flexible 3D stretch bending technology.

As shown in Fig. 1, the 3D bending machine consists of two symmetric ( $x$ - $z$  plane), semi bending arms. Five axes are implemented, thus providing each arm to have three degrees of freedom (DOF), namely: (1) one translation DOF governed by Axis 1 for the pre-/in-/post-process stretching; (2) one rotational DOF along  $y$ -direction at the  $x$ - $z$  plane, governed by Axis 2 - left and Axis 3 - right; and (3) another rotation DOF along  $z$ -direction at the  $x$ - $y$  plane, governed by Axis 4 - left and Axis 5 - right. The rotational DOF is realized by four rotational axes (pivots), installed in the base and the bilateral supports, respectively. The translation DOF is realized by the movement of the base platforms relative to each other. Axes 4 and 5 are controlled by hydraulic servo actuators and linear absolute encoders, whereas axes 2 and 3 are utilizing electric servos and rotary absolute encoders to ensure high positional accuracy during operation.

Two hydraulically-controlled clamp units are installed at the extreme end of each forming arm. A gripping pattern is machined on the surfaces of the clamp to provide enough traction, hence avoiding any slippage during stretch forming. The forming dies are mounted as inserts attached to the two pivoting semi die arms, in which the former can be flexibly

designed to accommodate the actual cross-section of the profile and the overall geometry of bent part. The entire bending operation is controlled by two rotational movement and one translational movement through the five axes. By controlling the different rotational axes, 2D and 3D bending geometries can be achieved. Based on the above-described method, a full-scale 3D stretch bending machine is developed, built and installed in a laboratory, as shown in Fig. 3.

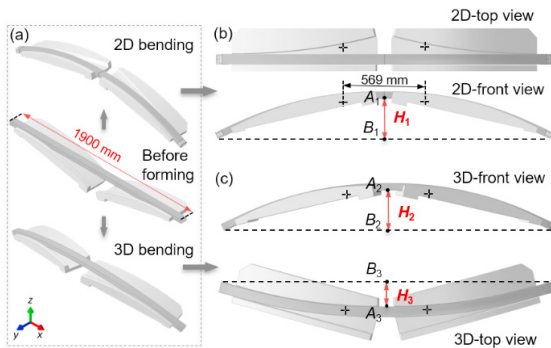


Fig. 2. Schematic view of the flexible stretch bending process and formed parts: (a) overview; (b) 2D bending; (c) 3D bending.



Fig. 3. Laboratory-based flexible, 3D stretch bending machine system.

### 3. Experiment and FE Modeling

#### 3.1. Experiment

AA6082-T4 extruded rectangular, hollow profiles are used in the experiments. The width of the profile is 60 mm, the depth is 40 mm, the gauge thickness is 3 mm, and the outer and inner fillet radii are 2 mm and 1 mm, respectively. By conducting tensile tests of samples cut from the middle zone of the top and bottom of the profile, the mechanical material properties are obtained as follows: Young's modulus is 71,982 MPa, the 0.2% offset proof stress (initial yield stress) is 146 MPa, the ultimate tensile strength is 266 MPa, the hardening exponent ( $n$ ) fitted by Swift equation is 0.26, and the normal anisotropy ( $r$ -value) is 0.34.

Both 2D and 3D bending experiments are carried out to verify the capabilities of the forming process and machine system. The initial length of the extrusion is 1,900 mm. The formed geometry shapes are shown in Fig. 2. The forming process includes three steps; viz., forming (bending), backward

movement (1<sup>st</sup>-stage unloading), and removal of tools (2<sup>nd</sup>-stage unloading). The backward moving is controlled in the  $x$ -direction (see Fig. 1) and the distance of movement is to partially release tension of the formed part, thus avoiding unintentional damage of machine and/or tools. As the backward movement cause longitudinal strain release of magnitude less than 0.0005, this process stage is entirely within the elastic domain, thus defined as 1<sup>st</sup>-stage unloading and the tooling removal as 2<sup>nd</sup>-stage unloading. The two unloading stages collectively lead to the global springback of the formed profile. For 2D bending, there is no imposed translation in  $y$ -direction during the bending process, which means that the whole process can be described as “bending → 1<sup>st</sup>-unloading → 2<sup>nd</sup>-unloading”. For the 3D bending, an additional stretching imposed by translational movement of the tools a total distance of 4 mm apart ( $y$ ) is proportionally applied along with the rotation of the two semi-die arms. Thus, the entire process can be described as “bending + stretching → 1<sup>st</sup>-unloading → 2<sup>nd</sup>-unloading”. Fig. 4 illustrates the experimental samples which were formed under the above-described 2D and 3D bending conditions.

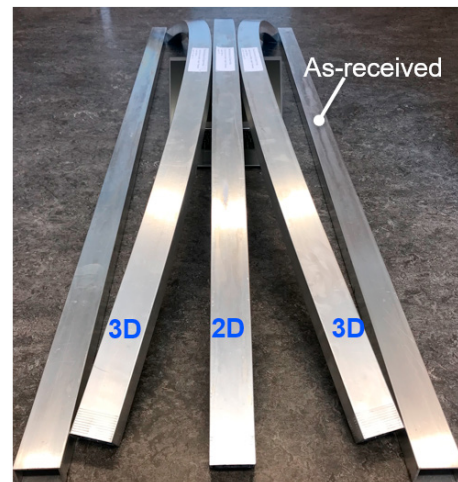


Fig. 4. Experimental 2D and 3D bent profiles.

#### 3.2. Numerical Modeling

In order to study the deformation characteristics of the forming process, FE analyses are carried out. Based on the experimental setup, the full process simulation of forming and elastic unloading is carried out using the commercially available FE program, Abaqus R2017x. Due to the complex contact conditions between tools and profile, the model would typically experience convergence problems by using an implicit solver. Thus, the bending step and reversing translational step are modeled in the Abaqus explicit solver. For the final unloading step (2<sup>nd</sup>-unloading), however, there is no external constraint caused by tools in the deformed part. Consequently, the final unloading step is modeled in the Abaqus implicit solver to ensure more accurate prediction of the final stress release step.

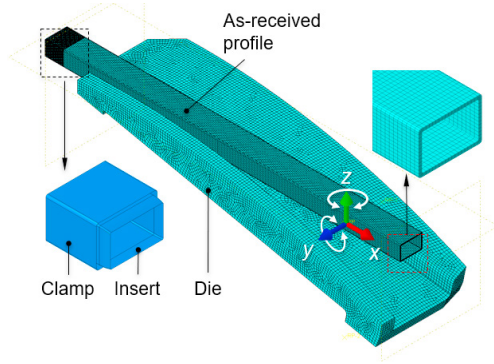


Fig. 5. FE model of 3D stretch bending process.

As shown in Fig. 5, due to symmetry, only the half model is employed to reduce computation time. The forming die, clamp tool, and inserts are modeled as discrete, rigid bodies. Considering the small ratio (less than 20) of width/depth-to-thickness and the large bending radii, the aluminum alloy profile is considered as a 3D deformable solid. The C3D8R brick element is used to mesh the profile instead of shell element, as the second alternative. The element size is the  $4 \times 3 \times 1$  mm (length  $\times$  width  $\times$  height). This implies that three elements are used across the thickness of the members of the profile, enabling a full observation of the stress/strain distribution including through-thickness stress. For the rigid bodies, the R3D4 element is employed to mesh the rigid die and clamp tools. The friction coefficient between the profile and the forming dies is set as 0.05. Loading velocity/time is not scaled and thus set the same as used in the experiments, namely, 8 seconds for bending and 2 seconds for the translational reversal movement. For the simulation of unloading, the formed profile and its deformation information are imported from the explicit simulation step (bending + backward moving). As the final unloading process is a free release process of elastic deformation energy without constraints of tools, only one node in the symmetry surface is fully constrained to avoid rigid body movement. It should be mentioned that a material orientation (local coordinate system) is defined as the same as the global coordinate system, in which  $x$ ,  $y$ , and  $z$  represent the longitudinal, transversal (width) and vertical (height) directions, respectively. Young's modulus and true plastic stress-strain curves obtained in Section 3.1 are used as the input of material elastic-plastic property in the FE modeling.

## 4. Results and Discussion

### 4.1. Dimensional Accuracy of Formed Profiles

The dimensional accuracy of the formed profile is determined by measuring the change between the actual geometry dimensions after springback and the same dimension determined by the forming dies at select reference points. Here, as shown in Fig. 2 (b), we define the distance ( $H_i$ ) between the midpoint (point  $A_1$ ) of the interior face and midpoint (point  $B_1$ )

of the end-to-end straight line as the index to examine the accuracy in 2D bending. Similarly, for 3D bending, as shown in Fig. 2 (c),  $H_2$  and  $H_3$  are used to characterize the deformation in two directions, respectively.

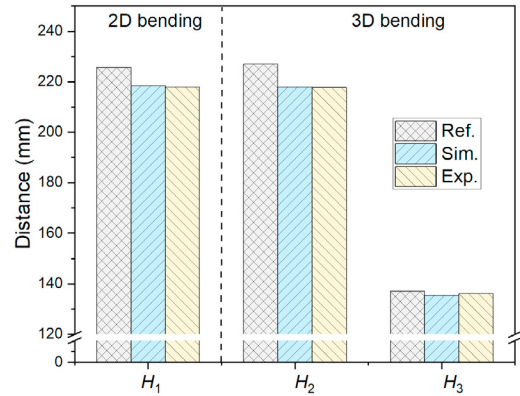


Fig. 6. Comparison between springback simulation and experimental results.

Fig. 6 illustrates experimental and FE simulation results, as well as the reference geometry dimensions of the part/tool before unloading. It can be seen that there is an obvious difference between experiments and reference chord heights of the samples, which we denote the elastic springback distance. Here, the springback magnitude distances with regard to experiment and simulation are defined as follows:

$$\Delta H_i^{\text{exp}} = H_i^{\text{ref}} - H_i^{\text{exp}} \quad (1)$$

$$\Delta H_i^{\text{sim}} = H_i^{\text{ref}} - H_i^{\text{sim}} \quad (2)$$

where  $\Delta H$  means the springback distance; the superscript 'ref' represents the reference dimension of the forming tools, and the superscripts 'exp' and 'sim' denote the experiment and simulation, respectively; the subscript  $i$  represents different reference positions, as shown in Fig. 2, where  $i=1$  refers to 2D bending, and  $i=2$  and  $i=3$  refer to the two bending directions in  $x$ - $z$  plane and  $x$ - $y$  plane, respectively, in the 3D bending case.

Accordingly, the relative error  $e(\Delta H_i)$  of springback prediction can be calculated by Eq. (3):

$$e(\Delta H_i) = \left| \frac{\Delta H_i^{\text{exp}} - \Delta H_i^{\text{sim}}}{\Delta H_i^{\text{exp}}} \right| \times 100\% \quad (3)$$

As shown in Fig. 6, the springback distance in the 2D bending case can be up to 7.11 mm. In the 3D bending case, the springback distances  $\Delta H_1^{\text{exp}}$  in  $x$ - $z$  plane, and  $\Delta H_2^{\text{exp}}$  in  $x$ - $y$  plane are 9.00 mm and 1.00 mm, respectively. Furthermore, by comparing the experiment with simulation, the relative error of springback prediction of 2D bending is  $e(\Delta H_1) = 7.03\%$ , and the relative errors of 3D bending with respect to two bending directions are  $e(\Delta H_2) = 3.67\%$  and  $e(\Delta H_3) = 12.00\%$ , respectively. It can be seen that the springback values predicted by the numerical model are close to the experimental results,

indicating good overall prediction capability. Therefore, in the next section, based on the full-process FE simulation, the deformation characteristics during bending process and the springback behaviors in 2D and 3D bending are analyzed.

#### 4.2. Characteristics of Bending Deformation

First, the deformation characteristics during 2D bending are analyzed. Fig. 7 (a) shows the von Mises stress distributions of the formed profile before 1<sup>st</sup>-stage unloading in 2D bending. As the bending deformation mainly occurs in the longitudinal direction, the longitudinal stress component S11 is analyzed in detail here. Note that in the following, all the stress/strain analyses are based on the material orientation (local coordinate system), as defined in Section 3.2, in order to intuitively reflect of stress/strain of different material points. It is observed that the entire bent profile is in a state of tension. Even at the interior face of the profile, the minimum S11 reaches about 140 MPa, which is close to the initial yield strength of the material. Thus, the location of the ‘neutral surface’, although from a theoretical perspective, is somewhere inside the two semi-die arms.

As mentioned in Section 3.1, there is no additional translation in the  $x$ -direction causing any movement of the semi dies apart, applied in the 2D bending. Thus, the stress state is entirely induced by the rotational movement of the two semi bending arms about the  $y$ -axis. In fact, the forming operation in this work resembles rotary draw bending, in which the clamp tools, pivot point and forming die (height) create a combination of bending and stretching as the two semi dies pivot around the  $x$ -axis, resulting in a state of tension within the entire part.

Fig. 7 (b) shows the equivalent plastic strain distribution of the bent part. As the deformation mainly occurs in the longitude direction, there is no obvious difference between the effective plastic strain (PEEQ) and longitudinal plastic strain component (PE11). The maximum PE11 at the external face is about 0.035 and the minimum PE11 at the interior face is near to zero. The plastic strain in the longitudinal direction is non-uniform; i.e., the closer to the middle zone of the whole profile (symmetric surface), the larger plastic strain. Across the depth of the section, the strain gradient is more pronounced in the region close to the symmetry plane ( $y$ - $z$ ). Ensuring a state of tension within the whole bent profile does reduce the internal bending moment ( $M_x$ ) along the entire part, thus reducing the springback upon unloading. Here, the tension imposed by rigid body kinematics of the semi dies can also be adjusted by superimposing longitudinal translation by moving the semi dies further apart (controlled by axis 1 as shown in Fig. 1), increasing stretching during bending process. Thus, this provides an opportunity to help minimize springback for improving the global dimensional accuracy of the formed component, within the constraints of the formability of the material and formation of local distortions.

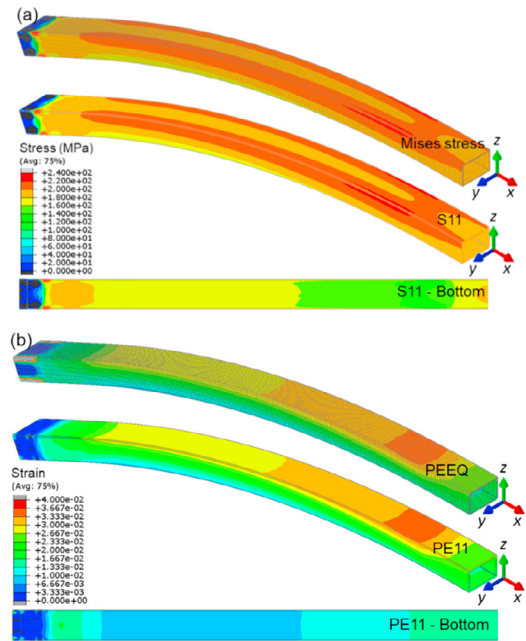


Fig. 7. Deformation characteristics of 2D bending: (a) stress distribution; (b) strain distribution.

Furthermore, the forming characteristics of 3D bending are to be discussed in the continuation. As shown in Fig. 8, the stress and strain distributions resemble superposition of the bending deformations in two perpendicular directions; in  $x$ - $z$  plane and  $x$ - $y$  plane, respectively. The maximum value of the strain component S11 reaches about 260 MPa, located at the middle zone of the intersection of extrados of the two bending axes. The minimum value of the stress component S11 is about 30 MPa, located at the interior corner next to the middle zone of the intersection of intrados of the two bending axes. Thus, the entire 3D bent profile is in a state of tension.

It can be seen from Fig. 8 (b) that the maximum plastic strain component PE11 reaches 0.06. The minimum PE11 vanish, approaching close to zero. As mentioned in Section 3.1, a backward movement (stretching) of 4 mm is imposed during bending, which creates about 0.002 additional plastic strain, as compared to keeping the semi dies at a fixed distance upon rotation. As this additional tensile strain is very low, it should not significantly affect the distributions of strain and stress. Owing to the superposition effect of deformations in dual axes bending, the non-uniform strain/stress gradients across the depth and along the profile are more pronounced in 3D than in 2D bending. However, it is to be noted that the deformation behavior of 3D stretch bending is more complex than would be the case of a simple linear superposition. For example, the cross-section will undergo local distortions, and the thickness variation will be more pronounced due to mass conservation under a complex 3D stress state.

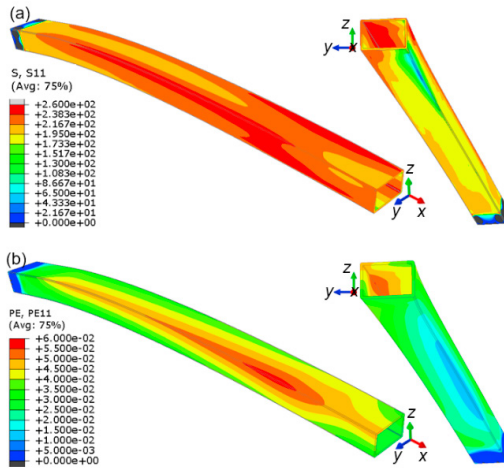


Fig. 8. Deformation characteristics of 3D bending: (a) stress distribution; (b) strain distribution.

### 4.3. Characteristics of Springback

Figs. 9 and 10 illustrate the springback characteristic of 2D bending. As mentioned above, the unloading process consists of two stages. The 1<sup>st</sup>-stage unloading is just a reverse movement of 1 mm in  $x$ -direction, releasing some pressure before the removal of tools. For the 2<sup>nd</sup>-stage unloading, as shown in Fig. 9, the maximum displacement with respect to  $x$ -direction and  $z$ -direction in the global coordinate system can be up to -1.22 mm and 7.82 mm, respectively. The ratios of the displacement components in  $x$ - and  $z$ -directions of total springback (including 1<sup>st</sup>-stage unloading and 2<sup>nd</sup>-stage unloading) to their corresponding reference distances are 0.13% and 3.48%, indicating that the springback in  $z$ -direction of the bent profile is much larger than that in  $x$ -direction. Fig. 10 (a) and (b) show the residual stress distribution after the two unloading stages. During the 1<sup>st</sup>-stage unloading, the maximum stress component S11 of the extrados can be reduced from about 240 MPa to 150 MPa, and the minimum S11 of intrados is reduced from about 130 MPa to 50 MPa, indicating a significant release of internal stress. When the external tools are removed, the maximum S11 is reduced to 15 MPa. For the intrados, however, the stress state changes from tension to compression, approaching about -30 MPa. The overview of tensile and compressive residual stress distribution is shown in Fig. 10 (c), showing that the compressive residual stress does not only occurs in the area near to the intrados, but also in the area of the external surface. In addition, the residual stress across the thickness does change from positive to negative, or from negative to positive in some areas. This implies that the 2<sup>nd</sup>-unloading leads to a local compressive and tensile residual stresses across the depth of the cross-section of the formed profile, in which the stress resultant maintains force equilibrium at any section along the length of the profile.

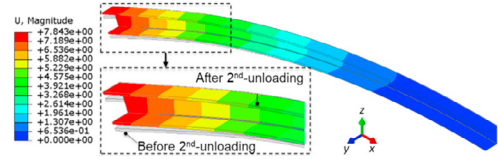


Fig. 9. Springback displacement in 2D bending.

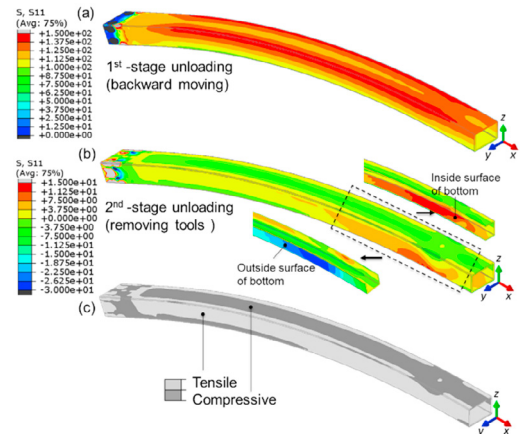


Fig. 10. Evolution of residual stress during springback in 2D bending: (a) after 1<sup>st</sup>-unloading; (b) after 2<sup>nd</sup>-unloading; (c) overview of tensile and compressive residual stress.

For 3D bending, a spatial springback phenomenon does occur. Fig. 11 shows the springback magnitude upon 2<sup>nd</sup>-stage unloading. The maximum springback magnitudes in  $x$ -,  $y$ - and  $z$ -directions in the global coordinate system during 2<sup>nd</sup>-stage unloading are  $[U_1, U_2, U_3] = [-1.95, 9.93, 2.03]$  mm, whose ratios to their corresponding total reference distances are -0.21%, 4.38%, and 1.48%, respectively. For the residual stress after complete unloading, as shown in Fig. 12, the stress concentration in the corner zone of the intersections is severe. At the intrados, in particular, there is a pronounced concentration of compressive stress, occurring at the corner near to the middle zone. The maximum compressive residual stress is reaching about -120 MPa. The pronounced compressive residual stress is caused by the severe non-uniform 3D deformation behavior represented by dual axes bending. Even though there is an additional movement of the semi-die arms 4 mm apart during bending, this movement induced additional tensile strain is very low so that it should not cause obvious effect on the overall stress distributions. As shown in Fig. 7 (a), due to the superposition effect of bending deformation in dual axes bending, the stress gradients across the depth and along the length of the 3D formed profile are more significant than those of the 2D formed profiles, which influence the residual stress distribution after unloading.

It is obviously more difficult to control the spatial springback phenomenon. From the point of springback minimization, the internal moments ( $M_x$  and  $M_y$ ) of the cross-section mainly determines the springback magnitude. For the

3D bending problems, however, the bending deformation in two perpendicular directions makes the stress gradient of the cross-section asymmetric. Moreover, the stress distribution changes significantly along the longitudinal direction of the component. This makes the 3D deformed part unload non-proportionally with respect to the different directions in the 3D space. Accordingly, there exist mutual constraints among different directions in deformed material in the global unloading process, making the distribution of residual stress after springback trend to be more complex than in 2D case.

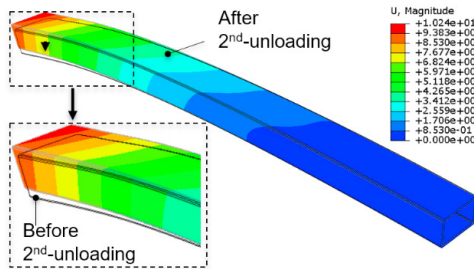


Fig. 11. Springback displacement in 3D bending.

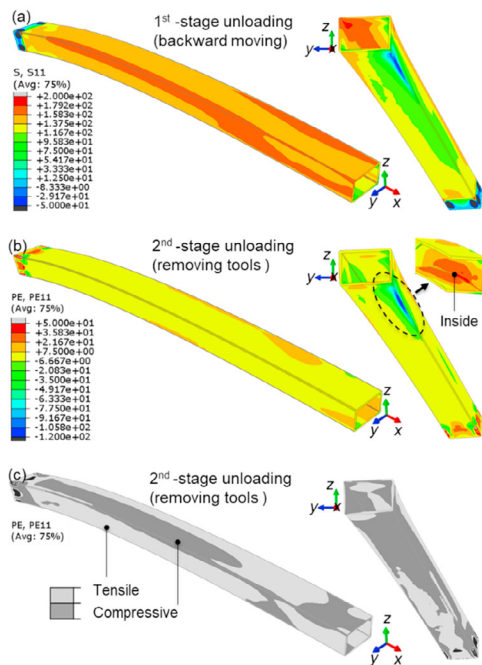


Fig. 12. Evolution of residual stress during springback in 3D bending: (a) after 1<sup>st</sup>-unloading; (b) after 2<sup>nd</sup>-unloading; (c) overview of tensile and compressive residual stress.

To reduce springback, the most important factor is to reduce the internal moment of the cross-section through reduced local S11 stress gradient across the depth of the cross-section. Applying sufficient simultaneous stretching upon bending can realize this purpose. If the additional stretching is too high, however, this may cause severe thinning and/or cross-sectional distortions, and/or formability problems of the material at the

external face of the profile. In addition, the proportionality of the stretching sequence, aiming to maintain continued loading upon stretching—and vice versa—can affect the moment distribution of the bent profile, and further change the springback magnitude. These issues need a more in-depth study to search for more optimal stretching and bending kinematics with regard to effective control of springback.

## 5. Conclusions

Motivated from the need to improve flexibility in manufacturing of complex profiles, this paper introduces a new, flexible 3D stretch bending process. Using experimental and numerical approaches, the capabilities of the forming method and machine are verified, and the characteristics and mechanisms are thoroughly explored to provide in-depth understanding of the forming process. The main conclusions can be drawn as follows:

- The innovation of the new, flexible 3D stretch bending is based on multi-axis design combined with a novel tooling concept utilizing part-specific inserts to enable the manufacture of complex geometrical configurations with low tool investments and multi-sensor integration, thus providing possibilities for real-time, in-process detection and control of the manufacturing process.

- The feasibility and capability of the new flexible stretch bending process are successfully verified in both 2D and 3D bending cases, using extruded aluminium alloy profiles. A full-process FE model is established and experimentally verified to analyze the combined bending-unloading process in detail. Both experiment and simulation indicate that the springback significantly affects geometrical accuracy of bent profiles.

- The characteristics of the bending process and the springback behaviors in 2D/3D bending are numerically studied. The forming process can provide a combination of stretching and bending during forming process, kinematically controlled by multi-DOF tooling movements, thus making the entire bent parts in a state of tension before unloading, without applying translational movement for additional stretching. The flexibility of bending kinematics of the 3D stretch bending machine provides a good basis for minimizing springback and maximizing accuracy through optimal control.

## Acknowledgements

The authors would like to thank the financial support from Norwegian University of Science and Technology (NTNU), NTNU Aluminium Product Innovation Center (NAPIC) and the KPN project VALUE (No. 267768) sponsored by Research Council of Norway, Hydro and Alcoa.

## References

- [1] Yang DY, Bambach M, Cao J, Duflou JR, Groche P, Kuboki T, Sterzing A, Tekkaya AE, Lee CW. Flexibility in metal forming. *CIRP Ann* 2018;67(2):743-765.
- [2] Allwood JM, Duncan SR, Cao J, Groche P, Hirt G, Kinsey B, Kuboki T, Liewald M, Sterzing A, Tekkaya AE. Closed-loop control of product properties in metal forming. *CIRP Ann* 2016;65(2):573-596.

- [3] Schjøtt-Pedersen N, Welo T, Ringen G, Raknes CA. Using set-based design for developing a 3D metal forming process. *Procedia CIRP*. 2019;84:149-154.
- [4] Welo T, Widerøe F. Precision bending of high-quality components for volume applications. *Trans Nonferrous Met Soc China*. 2010;20(11):2100-2010.
- [5] Li H, Ma J, Liu BY, Gu RJ, Li GJ. An insight into neutral layer shifting in tube bending. *Int J Mach Tools Manu* 2018;126: 51-70.
- [6] Yang H, Li H, Zhang ZY, et al. Advances and trends on tube bending forming technologies. *Chinese J Aeronaut* 2012;25(1): 1-12.
- [7] Chatti S, Hermes M, Tekkaya AE, Kleiner M. The new TSS bending process: 3D bending of profiles with arbitrary cross-sections. *CIRP Ann* 2010;59(1):315-318.
- [8] Staupendahl D, Tekkaya AE. The reciprocal effects of bending and torsion on springback during 3D bending of profiles. *Procedia Eng* 2017;207:2322-2327.
- [9] Holstein V, Hermes M, Tekkaya AE. Analysis of incremental die bending of wires and tubes. *Production Eng* 2020;29:1-10.
- [10] Ancellotti S, Fontanari V, Slaghenaufi S, Cortelletti E, Benedetti M. Forming rectangular tubes into complicated 3D shapes by combining three-roll push bending, twisting and rotary draw bending: the role of the fabrication loading history on the mechanical response. *Int J Mater Form* 2019;12(6):907-926.
- [11] Welo T, Baringsbing HA. On the evaluation of dimensional accuracy in rotary stretch bending. *Int J Mater Form* 2009;2(1):849-852.
- [12] Paulsen F, Welo T. Application of numerical simulation in the bending of aluminium-alloy profiles. *J Mater Process Technol* 1996;58:274-285
- [13] Liang JC, Gao S, Teng F, Yu PZ, Song XJ. Flexible 3D stretch bending technology for aluminum profile. *Int J Adv Manuf Technol* 2014;71(9-12):1939-1947.
- [14] Gao S, Liang JC, Li Y, Hao ZP, Li QH, Fan YH, Sun YL. Precision forming of the 3D curved structure parts in flexible multi-points 3D stretch bending process. *Int J Adv Manuf Technol* 2018;95(1-4):1205-2013.
- [15] Zhou Y, Li P, Li M, Wang L. Application and correction of L-shaped thin-wall aluminum in flexible-bending processing. *Int J Adv Manuf Technol* 2017;92(1-4):981-988.